CrossMark

Excellent electrochemical performance of graphene–polyaniline hollow microsphere composite as electrode material for supercapacitors

Hongfang Jiu[1] · Changshui Huang[1] · Lixin Zhang[2] · Jianxia Chang[1] · Hongqian Jiao[1] · Shaomei Zhang[1] · W. B. Jia[1]

Abstract The novel reduced graphene oxide–polyaniline hollow spheres (rGO–PANI HS) composite material has been prepared by a simple electrostatic interaction induced coassembly of graphene and PANI hollow microspheres (PANI HS). PANI HS about 800 nm in diameter have been synthesized utilizing PS spheres as hard templates after etching the templates, and hollow PANI@GO is reduced in hydrazine hydrate. The morphology and microstructure of the obtained samples have been characterized by XRD, FTIR and TEM. Furthermore, the performance of the rGO–PANI HS composites as supercapacitor electrodes material has been investigated. The composite has a specific capacitance of 752 F g^{-1} in 1 M H$_2$SO$_4$ solution. Furthermore, the capacitance of the rGO–PANI HS composite maintains 92 % after 500 charging/discharging cycles at a current density of 1 A g^{-1}, indicating a good cycling stability. The results suggest that rGO–PANI HS composite as novel electrode materials may have potential applications in high-performance energy storage devices.

1 Introduction

Supercapacitors, as important devices in energy storage and conversion systems, have increasingly attracted considerable attention in recent years because of high power density, fast charging/discharging processes (within seconds), and long cycle life [1–6]. However, the disadvantages of low energy density and high production cost have also restricted the rapid development of supercapacitors. It is urgent to make greater efforts in the design and synthesizing of novel materials for supercapacitor electrodes to resolve above obstacle. Graphene, an intriguing two-dimensional single-atom-thick carbon material, is an attractive electrode material for lithium ion batteries and electrochemical supercapacitor electrodes due to its extraordinarily high electrical and thermal conductivities, great mechanical strength, large specific surface area, and potentially low manufacturing cost [7–9]. PANIs have gained much attention because of their low cost, ease of synthesis, good environmental stability, and high specific capacitance from multiple redox states [10, 11]. Owing to high conductivity, high surface area, and ability to store energy, hybrids of graphene and PANI have offered great promise as supercapacitors electrode materials by the combination of the intriguing properties of graphene with those of PANI. Composites of PANI and graphene, graphite oxide, and graphene-based nanosheets or graphene paper have been successfully synthesized by situ chemical or electrochemical polymerization, covalent or noncovalent functionalization, and self-assembly method [12–17]. The PANI is in the forms of spheres, nanowires, nanofibers, or nanorods [18–22]. Especially, PANI with special nanostructure offers the possibility to enhance the electrochemical performance for supercapacitor application because of its greater exposure area and depth penetration for electrolyte ions. The unique nanostructures, like porous or hollow structures, provide particular advantages to supercapacitors due to the enhanced surface-to volume ratio and reduced transport lengths for both mass and charge transport [23, 24]. Owing to the unique properties, such as low

✉ Hongfang Jiu
  hongfangjiu@163.com

1 College of Science, North University of China, Taiyuan 030051, People's Republic of China

2 Chemical Engineering and Environment Institute, North University of China, Taiyuan 030051, People's Republic of China

density, high specific surface area, good permeation, good electrical conductivity and excellent electrochemical properties, PANI hollow spheres have drawn considerable interest recently [25, 26]. Hard-template methods have been widely adopted for the preparation of hollow structure materials since they are straightforward to apply and have obvious advantages for controlling the size, shape, and structure of shell [27]. However, the research work on the hollow structured PANI/graphene hybrids has seldom reported so far. Mu et al. [28] prepared Graphene/polyaniline hybrid hollow microspheres via combining layer-by layer assembly technique with in situ chemical oxidative polymerization after etching the templates for high-performance supercapacitor application. Liu et al. [29] synthesized the novel composites of graphene oxide-wrapped polyaniline hollow microsphere through a facile self-assembly method. Polyaniline hollow spheres@electrochemical reduced graphene oxide hybrids with core–shell structures have been fabricated via a solution-based coassembly process [30].

In this paper, the novel composite has been prepared by a simple electrostatic interaction induced coassembly of graphene and polyaniline hollow spheres (PANI-HS), followed by the hydrazine hydrate reduction of GO to rGO. The PANI-HS have been synthesized utilizing PS spheres as hard templates. The resulting samples were characterized by X-ray diffraction (XRD) and TEM. Furthermore, the performance of the graphene/polyaniline (PANI) composite as supercapacitor electrode material was investigated.

2 Experimental

2.1 Chemicals

Natural graphite powder (325 meshes) was purchased from Alfa-Aesar. Aniline and styrene were purchased from Tianjin Co.Ltd (Tianjin), ammonium persulfate (APS), tetrahydrofuran (THF), ethanol$\geqq$99.7 %, H_2SO_4, 30 %, H_2O_2, $KMnO_4$, $NaNO_3$, and 37 % HCl were supplied by China Medicine Co. Aniline and styrene were distilled under reduced pressure before use, and other reagents were used as received without further treatment. Deionized (DI) water was used throughout all the experiments.

2.2 Preparation of polyaniline hollow spheres (PANI-HS)

The negative charge monodispersed PS spheres with diameters of 1 μm were synthesized according to the procedures reported [31]. Then, a mixture of hydrochloric acid (2.5 M, 2 mL) and An (0.2 mL) was added to the above-

prepared PS (0.3 g) emulsions and stirred with a magnetic stirrer for 0.5 h in an ice/water bath to allow the swelling process and absorption of Aniline hydrochloride on the surface of the PS template spheres. Then, APS (equimolar quantities with An) dissolved in water was added immediately to the above mixture. The reaction was carried out in an ice/water bath for 8 h and left at room temperature for 16 h. The obtained products were washed repeatedly with deionized water and ethanol and finally dried in a dynamic vacuum at room temperature for 24 h.

The prepared PS/PANI composite microspheres were added into 50 mL of THF and stirred with a magnetic stirrer 25 °C for 24 h. Then centrifuged and washed with THF, and dried under vacuum 50 °C for 12 h to afford the PANI HS.

2.3 Preparation of graphite oxide (GO)

GO was prepared by a modified Hummers' method [32].In detail, 3 g graphite was put into a mixture of 15 mL H_2SO_4, 2.5 g $K_2S_2O_8$, and 2.5 g P_2O_5. The solution was heated to 80 °C and kept stirring for 5 h in water bath. Then the mixture was diluted with 700 mL water, filtered and washed. The product was dried under room temperature. Thereafter, 15.0 g $KMnO_4$ was slowly added with magnetic stirring, to prevent the temperature of the mixture from exceeding 10 °C by ice bath. The nice bath was then removed and the mixture was stirred at 35 °C for 2 h. The reaction was terminated by adding 800 mL of water and 25 mL H_2O_2 solution. The mixture was filtered and washed with 1:10 HCl aqueous solution to remove metal ions followed by DI water to remove the acid. Finally, the GO was obtained by drying.

2.4 Preparation of graphite oxide–polyaniline hollow spheres (GO–PANI HS) composite

GO was dispersed in water for further examination. PANI HS was diluted to 1 mg mL^{-1} with DI water under sonication for 0.5 h. Then, 24 mL of GO suspension (0.5 mg mL^{-1}) was added to 120 mL of hollow PANI suspension, and the resulting mixture was sonicated for another 2 h. After repeatedly centrifuging and washing with ethanol and water, the resultant product (GO–PANI HS) was collected and dried under vacuum at 40 °C for 12 h.

2.5 Preparation of reduced graphene oxide–polyaniline hollow spheres (rGO–PANI HS) composite

Hollow PANI@GO (100 mg) was dispersed in 150 mL of DI water sonicated for another 2 h, followed by reacting

with 3 mL of hydrazine hydrate at 95 °C for 3 h under stirring to yield a homogeneous suspension of rGO–PANI HS hybrids, The obtained products were washed repeatedly with deionized water and ethanol and finally dried in vacuum at 60 °C for 24 h.

2.6 Characterization

X-ray diffraction (XRD) patterns of the samples were conducted on an X'Pert Pro X-ray diffractometer with Cu Kα radiation (λ = 0.1542 nm) under a voltage of 40 kV and a current of 40 mA. Fourier transform infrared (FTIR) spectra were collected on a Nicolet Fourier spectrophotometer, using KBr pellets (Perkon-Elmer 1700, USA).Transmission electron microscopy (TEM) experiments were conducted on a JEOL 2011 microscope (Hitachi, Japan) operated at 200 kV. (Malvern, Zetasizer nanozs).

2.7 Electrochemical measurements

The electrochemical tests were carried out in 1 M H_2SO_4 aqueous electrolyte solution at room temperature. A three-electrode system was used, the samples were used as the working electrode, platinum as the counter electrode, and Ag/AgCl electrode as the reference electrode. Cyclic voltammetry (CV), galvanostatic charge/discharge curves, and electrochemical impedance spectroscopy (EIS) were performed with a CHI 660D electrochemical workstation (Chenhua Instruments Co., Shanghai, China). CV curves were collected at different scan rates in a range from −0.2 to 0.8 V, and galvanostatic charge/discharge curves were measured in a voltage ranging from 0 to 0.80 V. EIS was recorded in the frequency range from 105 to 0.01 Hz at open circuit potential with an alternating current (ac) voltage amplitude of 5 mV.

3 Results and discussion

3.1 The structure analysis of the GO, PANI HS and GO–PANI HS composite

XRD was employed to monitor the structure of samples. Figure 1 shows the XRD patterns of GO (a), PANI HS (b) and GO–PANI HS composite (c). The broad diffraction peak at 2θ = 9.4 corresponds to the typical diffraction peak of GO sheets, which is attributed to the introduction of oxygenated functional groups on carbon sheets (Fig. 1a). And the PANI HS have two broad peaks at approximately 2θ = 19.2° and 24.6° (Fig. 1b). The peak located at 2θ = 19.2° is due to the periodicity parallel to the PANI chains, while the 24.6° peak is ascribed to the periodicity
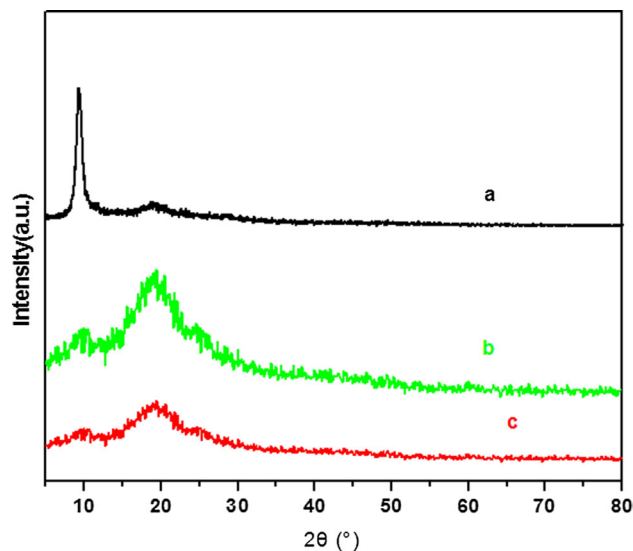

Fig. 1 XRD patterns of GO (*a*), PANI HS (*b*) and GO–PANI HS composite (*c*)

perpendicular to the PANI chains [29, 33]. It can be also seen that the XRD patterns of GO–PANI HS (Fig. 1c) and PANI HS samples are very similar, which indicates that no additional crystalline order has been introduced.

FTIR spectroscopy was used to further confirm the composition of samples. In the FTIR spectrum of GO (Fig. 2a), The strong band at around 3440 cm^{-1} is assigned to the stretching vibration of structural—OH groups. The characteristic peaks at 1730,1625,1399,1245, 1054 cm^{-1} are C=O stretching vibrations, C=C configurable vibrations from the aromatic zooms, C–OH stretching vibrations, C–O stretching vibrations of epoxy, C–OH stretching
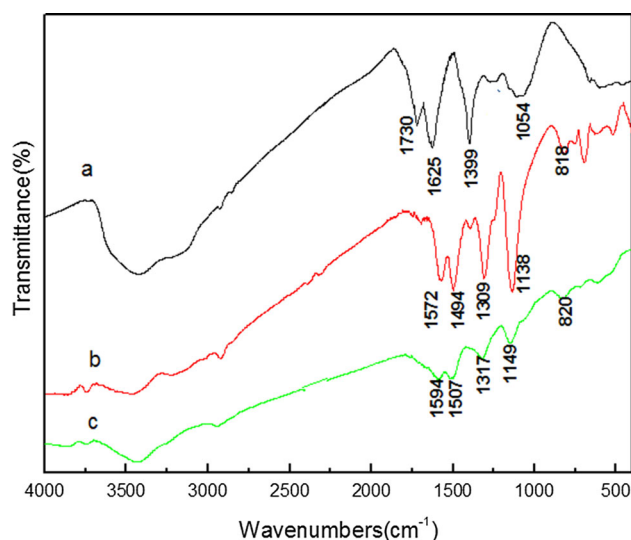

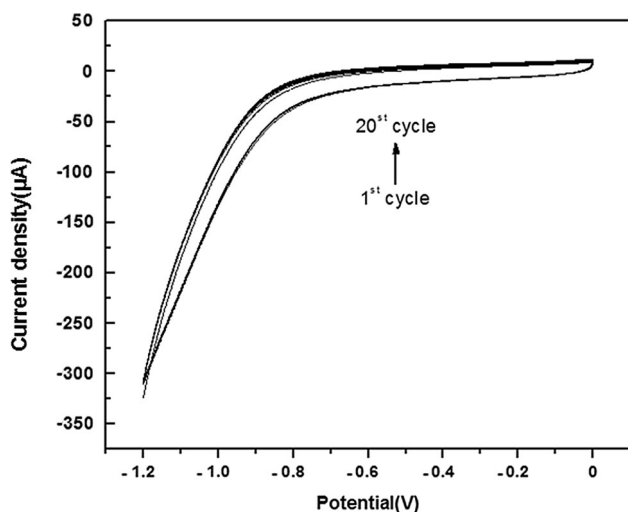**Fig. 2** FTIR of GO (*a*), PANI HS (*b*) and GO–PANI HS composite (*c*)

Fig. 3 CV curves of rGO–PANI HS composite at a scan rate of 50 mV s^{-1} in 0.2 M PBS (pH = 7)

vibrations [27]. In the FTIR spectrum of the PANI HS sample (Fig. 2b), the C=C stretching deformation of the quinoid (1572 cm^{-1}) and benzenoid rings (1494 cm^{-1}), C–N stretching of secondary amine in polymer main chain (1309 cm^{-1}), C–N stretching in bipolaron structure (1138 cm^{-1}), and out-of-plane deformation of C–H in the 1,4-disubstituted benzene ring (818 cm^{-1}) are observed [34]. By comparison, the resulting GO–PANI HS composite has similar characteristic bands as compared to the bands of pure PANI (Fig. 2c). However, some differences are noted from PANI HS. The peaks at 1138, 1309, 1494, 1572 cm^{-1} in PANI HS shift to higher frequencies of 1149, 1317, 1507, 1594 cm^{-1} in GO–PANI HS composite, respectively. The related high wavenumber of the FTIR peaks can be explained that the interaction between polyaniline chains and GO sheets restrict the modes of vibrations in polyaniline.

The cyclic voltammogram of rGO–PANI HS composite was performed in a potential range from 0.0 to −1.2 V at different cathodic potentials in PBS solution (phosphate buffered solution). The result (Fig. 3) shows that not found cathodic current peak, and the reduction peak was not produced during the whole cycle of scanning, which demonstrates that the reduction of surface-oxygenated species at GO in the composite was reduced to rGO in hydrazine hydrate completely.

3.2 The morphology of the GO, PANI HS and rGO–PANI HS composite

Figure 4 shows the TEM images of GO (a, b), PS microspheres templates (c), PS@PANI (d), PANI HS (e, f) and rGO–PANI HS (g, h). It can be seen from Fig. 4a, b that
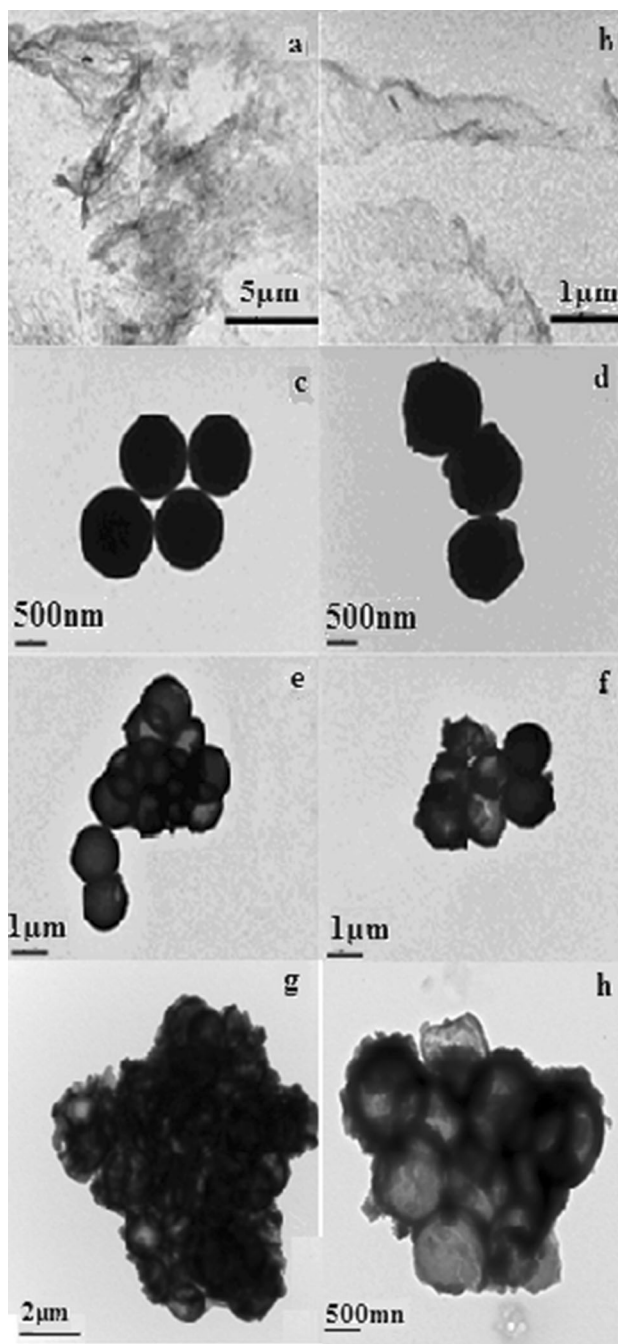

Fig. 4 Low (*left*) and high (*right*) magnification TEM images of GO (**a**, **b**); PS microspheres templates (**c**); PS@PANI (**d**); PANI HS (**e**, **f**) and rGO–PANI HS (**g**, **h**)

graphene sheets with visible wrinkles are of 2D lamellar structure, indicating the formation of the well-exfoliated graphene sheets [28]. The PS micospheres have an average diameter of 1 μm, whose surfaces are very smooth (Fig. 4c). From Fig. 4d, it is clear that the PS/PANI composite consists of solid spheres with an average diameter of 1.35 μm, which is much greater than that of the PS

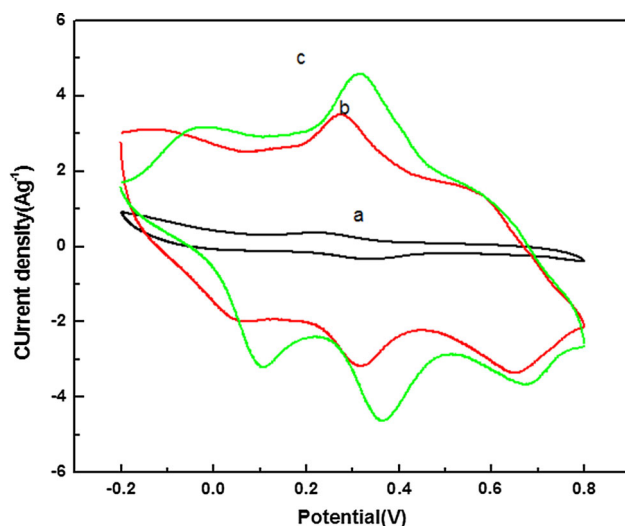**Fig. 5** CV curves of GO (*a*), PANI HS (*b*) and rGO–PANI HS composite (*c*) at a scan rate of 10 mV s^{-1} in 1 M H$_2$SO$_4$ solution

Fig. 6 CV curves of rGO–PANI HS composite at different scan rates of 10, 20, 50, and 100 mVs^{-1}, respectively

template spheres. The surface of the PS/PANI composite spheres becomes rough. This difference confirmed the formation of the PANI layer on the surface of PS spheres. The as-synthesized PANI hollow microspheres are fairly uniform in size (1.3 μm) and the shell thickness is approximately 100 nm (Fig. 4e, f). The strong contrast between the dark edge and the bright center can be observed in Fig. 4e, which indicates a hollow structure. The hollow sphere provides large specific surface areas enabling it to have particular advantage to electrochemical performance. Figure 4g and h show the TEM images of PANI-HS composite, and one can clearly observe the coexistence of PANI HS and graphene.

3.3 Electrochemical performance of the samples

Figure 5 demonstrated the CVs of GO, PANI HS and rGO–PANI HS composite at a scan rate of 10 mV s^{-1} in 1 M H$_2$SO$_4$ solution in the potential range from −0.2 to 0.8 V. From the CV curves shown in Fig. 5, the remarkable difference of electrochemical surface activity among GO, PANI HS and rGO–PANI HS composite can be easily recognized. The curve of GO electrode exhibits an approximately rectangular shape, indicating a typical electric double layer (EDL) capacitive behavior of the supercapacitor [35]. In a significant difference from GO electrode, both the PANI and the composite electrodes exhibit typical CV characteristic of PANI with two pairs of redox peaks, attributed to the redox transition of PANI between a semiconducting state (leucoemeraldine form) and a conducting state (polaronic emeraldine form) and transformation of emeraldine–pernigraniline [20, 21]. The CV curves of the rGO–PANI HS composite electrode presents the behavior of a combination of both redox and

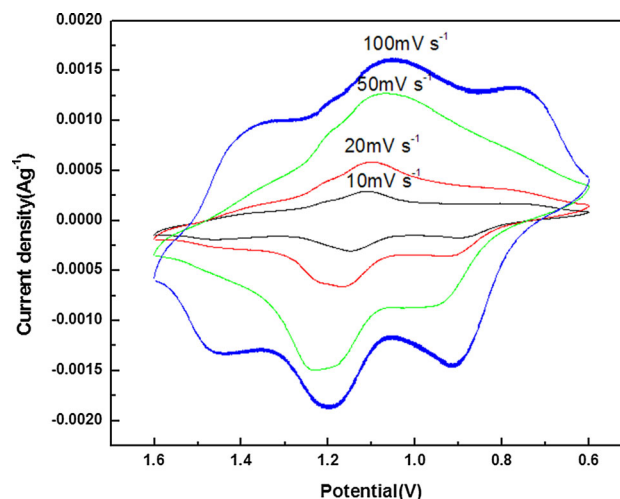EDL capacitance. When compared with pure PANI electrode, both the current density response of the rGO–PANI HS composite and the area surrounded by the CV curve are much larger, indicating higher specific capacitance. The PANI HS provide enhanced electrode/electrolyte interface area, which can enable the electrochemical accessibility of electrolyte through the packed PANI HS structure [10]. Furthermore, GO in the hybrids can not only offer highly conductive path, but also serve as a high surface area support material for PANI HS, facilitating rapid transport of the electrolyte ions in the electrode during rapid charge/discharge processes [23]. Therefore, the composites can greatly reduce the diffusion length, resulting in the improvement of electrochemical properties of rGO–PANI HS composites materials.

To further investigate the advantages of rGO–PANI HS composite at different scan rates, the rate-dependent cyclic voltammograms of the rGO–PANI HS composite electrode over a wide range of scan rates is shown in Fig. 6. It is obvious that the composite material exhibits excellent electrochemical performance in a wide range of scan rates. With increasing scan rate, the redox current increases clearly, indicating its good rate ability. The cathodic peaks shift positively, and the anodic peaks shift negatively with increasing the scan rates, which is mainly due to the resistance of the electrode [36].

The representative charge–discharge curves at a current density of 1 A g^{-1} are shown in Fig. 7. Specific capacitance was calculated by using Eq. 1, where I is the current loaded (A), Δt is the discharge time (s), ΔV is the potential change during discharge process, and m is the mass of active material in a single electrode (g).

$$C = \frac{I\Delta t}{\Delta V \times m} \tag{1}$$
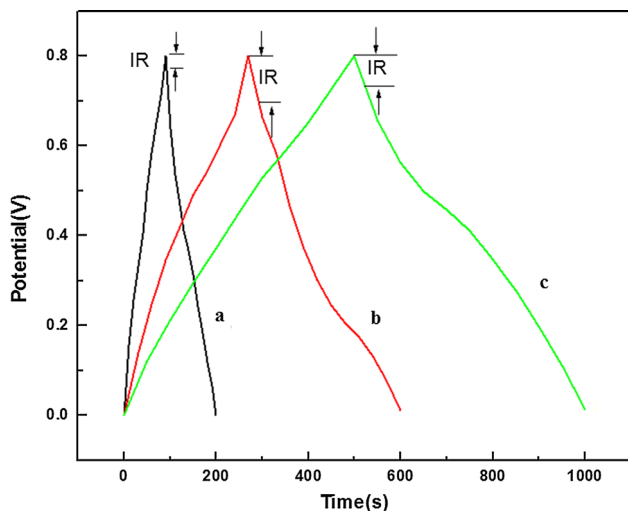
Fig. 7 Galvanostatic charge–discharge curves of GO (*a*), PANI HS (*b*) and rGO–PANI HS composite (*c*) within a potential window of 0–0.80 V at a current density of 1 A g^{-1}

Fig. 8 Plots of specific capacitance for PANI HS (*a*) and rGO–PANI HS composite (*b*) at various current densities

The GO electrode shows a triangular-shape charge–discharge curve, implying that its capacitance is mainly attributed to pure EDL capacitance. Obviously, the discharging curve of the rGO–PANI HS electrode is not ideal straight line and exhibits two voltage stages in the potential ranges of 0.8–0.45 and 0.45–0 V. The first stage is only associated with electric double-layer capacitance while the latter stage is ascribed to the combination of electric double-layer capacitance of graphene and the pseudocapacitance of PANI [10]. Furthermore, the IR drop of rGO–PANI HS is much lower than that of PANI HS, indicating that the introduction of rGO reduces significantly internal resistance. Because PANI in its leucoemeraldine or pernigraniline form is an insulator, the supercapacitor based on PANI HS has a large internal resistance in the charged or discharged process. GO greatly enhances the electronic conductivity of the hybrids by forming a conductive network between the adjacent PANI HS, which results in a low internal resistance. Thus, rGO–PANI HS composite is more suitable for power saving device.

Figure 8 displays the specific capacitance curves of PANI HS (a) and rGO–PANI HS composite (b) electrode materials at different current densities. The maximum specific capacitance value of PANI HS is calculated to be 521 F g^{-1}, while rGO–PANI HS exhibits higher specific capacitance values of 752 F g^{-1}. This could be attributed to the synergy effect between PANI HS and reduced graphene oxide. PANI nanoparticles provide a high capacitance; meanwhile, the reduced graphene oxide with good conductivity can avoid the agglomeration of PANI HS. Moever, the specific capacitance of the rGO–PANI HS composite material retains 63 % (from 752 to 475 F g^{-1}) as current density increases from 0.5 to 10 A g^{-1}, whereas
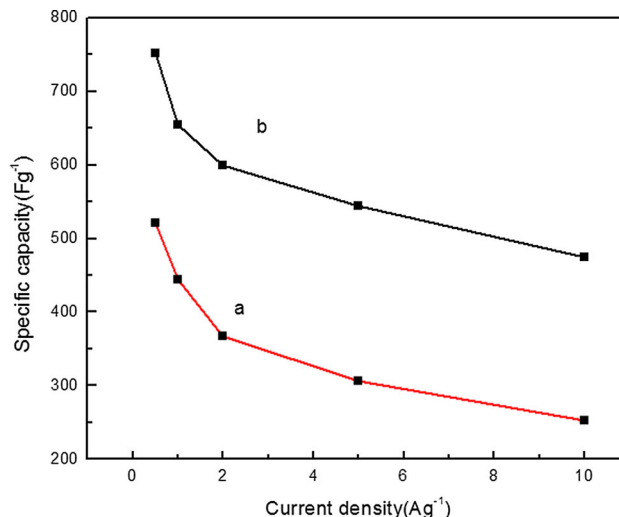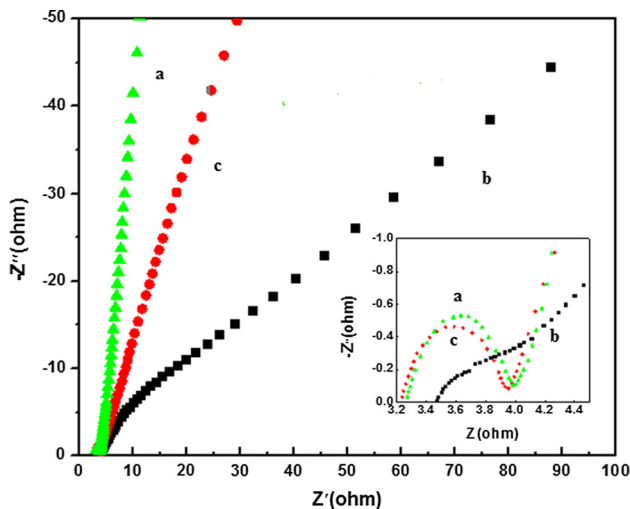

Fig. 9 Nyquist plots for GO (*a*), PANI HS (*b*) and rGO–PANI HS composite (*c*) electrodes. Z′, real impedance; Z″, imaginary impedance. The *inset* shows an enlarged scale

PANI HS keeps about 48 % of its capacity in the same current density range. This result is in good accordance with the CV tests.

The electrochemical impedance spectroscopy (EIS) analysis data were analyzed using Nyquist plots, which show the frequency response of the electrode/electrolyte system and are the plots of the imaginary component (Z″) of the impedance against the real component (Z′). The Nyquist plots of GO (a), PANI HS (b) and rGO–PANI HS composite (c) electrodes are displayed with the frequency range from 100 kHz to 0.01 Hz in Fig. 9. Both plots of the GO and PANI HS electrodes display a small semicircle at high frequency followed by a transition to linearity at low
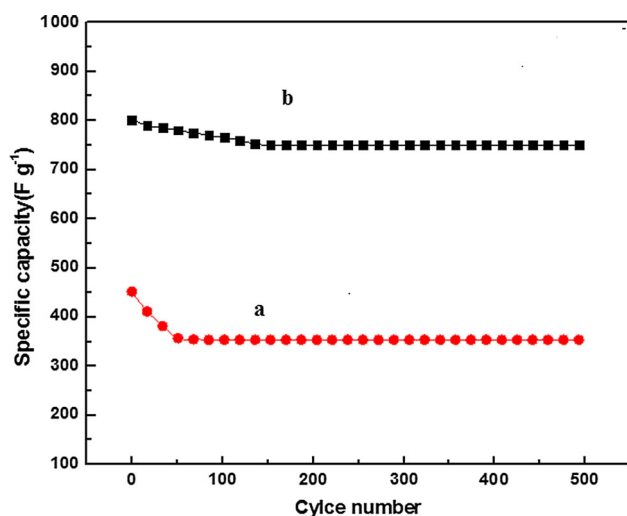
Fig. 10 Cycling stability of PANI HS (*a*) and rGO–PANI HS (*b*) composite upon charging–discharging at a current density of 1 A g^{-1}

frequency. The Nyquist plot of rGO–PANI HS composite electrode shows a straight line in the low -frequency region and an arc in the high-frequency region. At low frequency, the hybrid electrodes exhibit a more vertical line than neat PANI, showing a better capacitor behavior [37]. Impedance measurements can provide useful information about the equivalent series resistance (ESR) the electrode. The intersection of the plots at the X-axis represents the ESR of the electrode which determines the charge/discharge rate of the electrode [7]. As seen from Fig. 9, it is apparent that the ESR of GO, PANI HS and rGO–PANI HS composite electrodes is 3.26, 3.46, and 3.24 Ω, respectively. The smaller ESR of rGO–PANI HS composite than that of PANI HS may be attributed to the doping process and π–π stacking between GO and PANI HS, in which the structure can facilitate the efficient access of electrolyte ions to the electrode surface and shorten the ion diffusion path.

The instability of conducting polymers during the long-term charge/discharge processes is a detrimental issue in supercapacitor applications. The cycle stability of PANI HS and rGO–PANI HS composite was measured by long-term charge/discharge cycling at a current density of 1 A g^{-1} (Fig. 10). The capacitance of PANI HS lost almost 22 % (from 452 to 354 F g^{-1}) after 500 charging–discharging cycles. It is noted that the PANI HS shows the worst cycling stability (Fig. 10a), possibly resulting from the PANI HS undergoing swelling, shrinkage, cracking, or breaking, which induces gradual deterioration of the conductivity and volumetric changes [27]. During long-term charge/discharge cycling, the instability of the capacitors based on PANI is one of their most lethal deficiencies. However, retention of the specific capacitance is as high as 92 % of the initial capacitance after 500 cycles under the

same conditions. In the composite material, GO sheets provided a robust support for sustaining PANI HS, thus enhancing the mechanical strength of the composites and preventing the PANI from swelling and shrinking during the long-term cycling. Therefore, the graphene sheets can provide dual functions for improving the electrical conductivity and the stability of electrodes [30].

4 Conclusions

In summary, we have successfully synthesized the rGO–PANI HS composite by a simple electrostatic interaction induced coassembly of GO and PANI HS, followed by the hydrazine hydrate reduction of GO to rGO. The hollow structures of PANI HS by utilizing PS spheres as hard templates. The supercapacitor based on rGO–PANI HS electrode showed a high specific capacitance of 752 F g^{-1} at a current density of 1 A g^{-1} in 1 M H$_2$SO$_4$ solution. Moreover, the rGO–PANI HS electrode exhibited a good cycling stability and rate capability. The greatly enhanced specific capacitance is due to the synergic effect of the two components of rGO and PANI HS. Therefore, the composite is very promising in supercapacitors as well as other power source system.

References

1. D.C. Iwueke, C.I. Amaechi, A.C. Nwanya, A.B.C. Ekwealor, P.U. Asogwa, R.U. Osuji, M. Maaza, F.I. Ezema, J. Mater. Sci. Mater. Electron. **26**, 2236–2242 (2015)
2. A.S. Westover, J.W. Tian, S. Bernath, L. Oakes, R. Edwards, F.N. Shabab, S. Chatterjee, A.V. Anilkumar, C.L. Pint, Nano Lett. **14**, 3197–3202 (2014)
3. S. Dhibar, S. Sahoo, C.K. Das, R. Singh, J. Mater. Sci. Mater. Electron. **24**, 576–585 (2013)
4. Y. Lei, J. Li, Y.Y. Wang, L. Gu, Y.F. Chang, H.Y. Yuan, D. Xiao, ACS Appl. Mater. Interfaces **6**, 1773–1778 (2014)
5. M. Li, Y.Q. Zhang, L.L. Yang, Y.K. Liu, J.Y. Ma, J. Mater. Sci. Mater. Electron. **26**, 485–492 (2015)
6. S. Vijayakumar, S. Nagamuthu, G. Muralidharan, ACS Appl. Mater. Interfaces **5**, 2188–2196 (2013)
7. M.D. Stoller, S. Park, Y. Zhu, J. An, R.S. Ruoff, Nano Lett. **8**, 3498–3502 (2008)
8. Y. Wang, Z.Q. Shi, Y. Huang, Y.F. Ma, C.Y. Wang, M.M. Chen, Y.S. Chen, J. Phys. Chem. C **113**, 13103–13107 (2009)
9. J.R. Miller, R.A. Outlaw, B.C. Holloway, Science **329**, 1637–1639 (2010)
10. Q. Wu, Y.X. Xu, Z.Y. Yao, A. Liu, G.Q. Shi, ACS Nano **4**, 1963–1970 (2010)

11. H. Peng, G.F. Ma, W.M. Ying, A.D. Wang, H.H. Huang, Z.Q. Lei, J. Power Sources **211**, 40–45 (2012)
12. D.D. Xu, Q. Xu, K.X. Wang, J. Chen, Z.M. Chen, A.C.S. Appl, Mater. Interfaces **6**, 200–209 (2014)
13. D.W. Wang, F. Li, J.P. Zhao, W.C. Ren, Z.G. Chen, J. Tan, Z.S. Wu, I. Gentle, G.Q. Lu, H.M. Cheng, ACS Nano **3**, 1745–1752 (2009)
14. L. Zhao, L. Zhao, Y. Xu, T. Qiu, L. Zhi, G. Shi, Electrochim. Acta **55**, 491–497 (2009)
15. Y.M. Shulga, S.A. Baskakov, V.V. Abalyaeva, O.N. Efimov, N.Y. Shulga, A. Michtchenko, L. Lartundo-Rojas, L.A. Moreno-R, J.G. Cabañas-Moreno, V.N. Vasilets, J. Power Sources **224**, 195–201 (2013)
16. H. Gómez, M.K. Ram, F. Alvi, P. Villalba, E. Stefanakos, A. Kumar, J. Power Sources **196**, 4102–4108 (2011)
17. Y.F. Xu, I. Hennig, D. Freyberg, A.J. Strudwick, M.G. Schwab, T. Weitz, K.C. Cha, J. Power Sources **248**, 483–488 (2014)
18. N.A. Kumar, H.J. Choi, Y.R. Shin, D.W. Chang, L.M. Dai, J.B. Baek, ACS Nano **6**, 1715–1723 (2012)
19. J.J. Xu, K. Wang, S.Z. Zu, B.H. Han, Z.X. Wei, ACS Nano **4**, 5019–5026 (2010)
20. K. Zhang, L.L. Zhang, X.S. Zhao, J.S. Wu, Chem. Mater. **22**, 1392–1401 (2010)
21. J. Li, H.Q. Xie, Y. Li, J. Liu, Z.X. Li, J. Power Sources **196**, 10775–10781 (2011)
22. B. Ma, X. Zhou, H. Bao, X.W. Li, G.C. Wang, J. Power Sources **215**, 36–42 (2012)
23. J.S. Chen, Z.Y. Wang, X.C. Dong, P. Chen, X.W. Lou, Nanoscale **3**, 2158–2161 (2011)
24. H. Chen, S.X. Zhou, M. Chen, L.M. Wu, J. Mater. Chem. **22**, 25207–25216 (2012)
25. Y.Z. Long, Z.J. Chen, Y.J. Ma, Z. Zhang, A.Z. Jin, C.Z. Gu, L.J. Zhang, Z.X. Wei, M.X. Wan, Appl. Phys. Lett. **84**, 2205–2207 (2004)
26. K.C. Huang, C.W. Hu, C.Y. Tseng, C.Y. Liu, M.H. Yeh, H.Y. Wei, C.C. Wang, R. Vittal, C.W. Chucd, K.C. Ho, J. Mater. Chem. **22**, 14727 (2012)
27. J.J. Xu, K. Wang, S.Z. Zu, B.H. Han, Z.X. Wei, ACS Nano **4**, 5019–5026 (2010)
28. B. Mu, W.B. Zhang, A.Q. Wang, J. Nanopart. Res. **16**, 2432 (1–12) (2014)
29. M.C. Liu, X.L. Wu, C.L. Chen, Q. Wang, T. Wen, X.K. Wang, Sci. Adv. Mater. **5**, 1686–1693 (2013)
30. W. Fan, C. Zhang, W.W. Tjiu, K.P. Pramoda, C.B. He, T.X. Liu, ACS Appl. Mater. Interfaces **5**, 3382–3391 (2013)
31. L. Wang, H. Liang, F. Wang, L.Y. Huang, Z.P. Liu, Z.X. Dong, Langmuir **29**, 5863–5868 (2013)
32. J.W.S. Hummers, R.E. Offeman, J. Am. Chem. Soc. **80**, 1339 (1958)
33. C.A. Amarnath, J. Kim, K. Kim, J. Choi, D. Sohn, Polymer **49**, 432–437 (2008)
34. J. Han, P. Fang, J. Dai, R. Guo, Langmuir **28**, 6468–6475 (2012)
35. X.S. Cai, Q.L. Zhang, S.J. Wang, J. Peng, Y.W. Zhang, H.L. Ma, J.Q. Li, M.L. Zhai, J. Mater. Sci. **49**, 5667–5675 (2014)
36. Y.G. Wang, H.Q. Li, Y.Y. Xia, Adv. Mater. **18**, 2619–2623 (2006)
37. H.L. Wang, Q.L. Hao, X.J. Yang, L.D. Lu, X. Wang, ACS Appl. Mater Interfaces **2**, 821–828 (2010)